Journal of Stress Analysis
Vol. 2, No. 1, Spring – Summer 2017
Bu-Ali Sina University

Evaluation of SIF in FGM Thick-walled Cylindrical Vessel

N. Habibi*, S. Asadi, R. Moradikhah
Mechanical Engineering Department, University of Kurdistan, Sanandaj, Iran.

Article info

Article history:
Received 03 July 2017
Received in revised form
05 September 2017
Accepted 12 September 2017

Keywords:
FGM
BEM
Stress intensity factor
Pressure vessel
XFEM
FM

Abstract

In the present research, an internal semi-elliptical surface crack in a FGM thick-walled cylindrical vessel under internal pressure is assumed. The Poisson ratio is constant throughout the vessel and the material is considered to be isotropic with exponentially varying elastic modulus. The K_I is calculated using the BEM and FEM for different values of the relative depths of crack and material gradients. The research results show that increasing the E_2/E_1, decreases SIF and when $E_2/E_1 = 10$, the SIF of the FGM vessel is often lower than the corresponding homogeneous vessel. It can be observed that the relation between K_I and internal pressure in FGM is linear as for homogeneous materials, so that increasing internal pressure K_I increase as the same. The obtained results of BEM and FEM methods show that good agreement between the results can be seen.

Nomenclature

a	The major axe of the semi-elliptical crack	b	The minor axe of the semi-elliptical crack
A_b, A_i	System matrices	E	Elastic modulus
$C_{ij}(y)$	Coefficient dependent on the local boundary geometry at point y	Q	Elliptical crack front shape coefficient (square of the complete elliptical integral of the second kind)
E_1	Elastic modulus at the inner radius of cylinder	E_2	Elastic modulus at the outer radius of cylinder
f, F	A function and its radial integral	f_i	Traction vector
$F_{ij}^A, F_{ij}^1, F_{ij}^0$	Radial integrals	G	Strain energy release rate
G_c	Critical strain energy release rate	I	Identity matrix
K_I	SIF for opening mode	K_{II}	SIF for shearing mode
$\overline{K}_I$	Normalized SIF for opening mode	$\overline{K}_{II}$	Normalized SIF for shearing mode
K_0	Nominal K_I	N_b	Number of boundary nodes
N_{i_t}	Number of interior nodes	N_t	Number of total nodes
n_i	Outward unit normal vector	p	Internal pressure
R_o	The outer radius of cylinder	r	Distance $r = \|x - y$ on polar coordinat
R	Coordinate of the radial basis function	R_i	The inner radius of cylinder
$\overline{R}, \overline{R}_i$	Ancillary parameters in the radial integration method	s	Ancillary parameters in the radial integration method
U_{ij}	Displacement fundamental solutions	u_i	Displacement vector

*Corresponding author: N. Habibi (Assistant Professor)
E-mail address: n.habibi@uok.ac.ir
http://dx.doi.org/10.22084/jrstan.2017.14362.1026
ISSN: 2588-2597

$\overline{u}$	Normalized displacement vector	$\overline{u}_j$	Body force
V_{ij}	Traction fundamental solutions	V_b, V_i	System matrices
x, y, z	Cartesian coordinates	x	Field point
x^A	Application point	x_b	Vector of unknown boundary data
t	Thickness of cylinder	T_{ij}	Traction fundamental solutions
y	Source point	y_b	Vectors of known data on the boundary
y_i	Vectors of known data on interior node		node
Greek Symbols			
$\phi_i^A, \phi_i^k, \phi_i^o$	Coefficients in the approximation of the normalized displacements	β	Gradient parameter (the constant of material non-homogeneity)
Φ^A	Radial basis function	ν	Poissons ratio
μ	Shear modulus	$\overline{\mu}$	Normalized shear modulus
μ_{tip}	Shear modulus at the crack-front	φ	Parametric angle of an elliptical crack
δ_{ij}	Kronecker symbol	δ	Distance to the crack-front
$\Delta u_\xi, \Delta u_{\dot\eta}, \Delta u_\gamma$	Crack-opening-displacements (CODs)	$\xi, \dot\eta, \gamma$	Local coordinate system
Γ	Boundary of a domain	Ω	Analyzed domain
Abbreviations			
BDI	Boundary-Domain-Integral	BEM	Boundary Element Method
BEs	Boundary Elements	BIs	Boundary Integrals
CBT	Corrected Beam Theory	CCM	Compliance Calibration Method
CG	Crack Geometry	CODs	Crack Opening Displacements
CTOD	Crack Tip Opening Displacement	DI	Domain Integral
DIs	Domain Integrals	FEM	Finite Element Method
FGM	Functional Graded Material	FM	Fracture Mechanics
LEFM	Linear Elastic Fracture Mechanics	LES	Linear Elastic Solids
MG	Material Gradient	MGs	Material Gradients
RBF	Radial Basis Functions	RIM	Radial Integration Method
SIF	Stress Intensity Factor	SIFs	Stress Intensity Factors
VCC	Virtual Crack Closure	WFM	Weight Function Method
XFEM	Extended Finite Element Method		

1. Introduction

An FG material is a two-element composite defined by a compositional gradient from one element to the other. For instance, the FG ceramic/metal materials which combine the advantages of ceramics and metals. The distribution of each material changes continuously with space variables, which introduces non-homogeneity in the mechanical properties of these materials. Because of high mathematical complexity of the arising governing partial differential equations with non-constant coefficients, using analytical methods is so difficult for crack problems in FGMs in complex geometrical and loading conditions so numerical methods have been developed for modeling these problems. One of these methods is BEM. Although the BEM has been successfully applied to homogeneous cylindrical vessels, its application to FGM cylindrical vessels has been very limited. The effects of material distribution on K_I in cylindrical vessels and structures have been investigated from different methods. Seifi [1] applied the WFM for determination of SIF with internal surface cracks in an autofrettaged FG cylinders. Eshraghi and Soltani [2] estimated SIF for FG cylinders with internal circumferential cracks using the WFM.

Shaghaghi Moghaddam et al. [3] determined the mixed mode for SIF of 3D surface cracks in FGM hollow cylinders and studied the effect of Poisson's ratio and elastic modulus, which were defined by an exponential law in radial direction, on the SIF in detail. Afsar and Anisuzzaman [4] assumed a thick-walled FGM cylinder with two diametrically opposed edge cracks emanating from the inner surface; some numerical results of SIF were presented for different profiles of material distribution in the FGM cylinder. Ootao et al. [5] optimized the material distribution for the relaxation of thermal stresses in an FGM hollow sphere for thermal stress relaxation using the analytical procedure of a laminated hollow sphere model. They [6] also considered an FGM hollow cylinder and optimized the material distribution for thermal stress relaxation. Saidi et al. [7] presented analytically solutions for determination of displacement and stress components of thick-walled spherical FG vessels.

In the other research [8] a new method to determine the fracture properties and shear modulus (G) for carbon-polyester composite was introduced. Theoretical studies to determine G were conducted using three methods: CBT, CCM, and VCC Technique, and obtained results were compared with the results from

experimental and numerical attempts. EL-Desouky and EL-Wazery [9] obtained Zirconia-Nickel FGMs by powder metallurgy technique. Mixed-mode fracture response of YSZ/Ni FGMs was examined utilizing the three-point bending test and FEM. The obtained results indicated that the K_I and K_{II} for the FGM are less than those for non-graded composite under mixed mode loading conditions.

It is self-evident that the applications of FGM vessels are widespread. Pressure vessels are widely used in the aerospace, nuclear, chemical, and automobile industries. Due to this widespread use, vessels must operate under extreme mechanical loadings; any failure or fracture will be an irreparable disaster.

The opening mode SIF is calculated using the BEM developed by Zhang et al. [10], which uses an advanced BEM based on the boundary domain integral equation formulation in conjunction with a meshless method. Wearing and Ahmadi-Brooghani [11] studied the application of the BEM for determination of K_I in plate bending problems. A number of case studies having a range of plan forms, with different combinations of boundary conditions, crack configurations, and loading conditions were presented to illustrate the effectiveness of the BEM for the fracture analysis of plates. J-integral, displacement extrapolation, quarter point, and stress extrapolation were some methods used to determine the SIF. The BEM results for the case studies considered in the paper were compared with either analytical or FEM results and a good agreement was achieved.

The performance of several super convergent techniques to extract K_I from computed numerical solutions with the generalized FEM was investigated by Pereira and Duarte [12]. In the other study, Purbolaksono et al. [13] studied the normalized SIF for multiple semi-elliptical surface cracks on two surfaces (inner and outer) of tubes containing oxide scale on inner part. Tubes were subjected to internal pressure.

Barroso et al. [14] investigated an efficient post-processing procedure for the evaluation of multiple generalized K_I in multi-material corners according to BEM. The procedure is based on a simple least squares fitting using numerical results of displacements and stresses along boundary edges and the common edges of the wedges in a multi-material corner. A new extended dual BEM was presented by Alatawi and Trevelyan [15] in which the enrichment functions are based closely on the K_I in LEFM theory for 2D conditions. The method is able to evaluate SIF directly without any requirement of post-processing calculations such as the J-integral. Tutuncu and Ozturk [16] studied exact solution of deformation and stress in FGM spherical and cylindrical vessels under internal pressure. It was shown that having higher stiffness or elastic modulus near the inner surface leads to decrease in stresses through the wall thickness [16]. Horgan and Chan studied FGM shallow discs and cylinders with internal pressure with limited length [17].

Jabbari et al. [18] presented analytical solution for the calculation of the axisymmetric thermal and mechanical stresses in an FGM thick hollow cylinder. Ghasemi et al. [19] studied an FGM cylindrical shell reinforced by laminated composite subjected to internal pressure. In the other research, Elastic analysis was performed for two thick walled FGM spherical and cylindrical vessels by Chen and Lin [20]. The property of FGM was assumed to be in exponential function form. Abrinia et al. [21] presented new method for analysis of FGM thick-walled cylinders under combined thermal and pressure loading. It was assumed that elastic modulus and the coefficient of thermal expansion in FG materials in thickness direction is in exponential function form and Poissons ratio is constant.

It is observed, there is a limited amount of literature available on the application of BEM in cracked FGM cylindrical vessels. Therefore, in the present work, an FGM thick-walled cylindrical vessel with semi-elliptical surface crack under internal pressure is considered, also, Poissons ratio is constant throughout the material [21] and the material is assumed to be isotropic with exponentially varying elastic modulus [20].

2. The Boundary Domain Integral (BDI) Equations

For an isotropic, non-homogeneous and linear elastic solid with elastic modulus E(x) dependent on Cartesian coordinates and the constant Poisson's ratio, The BDI equations can be written as [10]

$$\overline{u}_i(y) = \int_\Gamma U_{ij}(x,y) f_j(x) d\Gamma - \int_\Gamma T_{ij}(x,y) \overline{u}_j(x) d\Gamma + \int_\Omega V_{ij}(x,y) \overline{u}_j(x) d\Omega \tag{1}$$

where, U_{ij} is displacement fundamental solution, and V_{ij}, T_{ij} are traction fundamental solutions respectively; Ω and Γ are the analysis and the boundary of domains respectively. Furthermore, $u_i(x)$ and $f_i(x)$ are displacements and tractions at point p on boundary Γ; x and y denote the source point and the field point respectively. The functions of $\overline{u}_i(x)$ and $\overline{\mu}(x)$ are the normalized displacements and shear modulus respectively, which can be shown as below:

$$\overline{u}_i(x) = \mu(x) \cdot u_i(x) \tag{2}$$

$$\overline{\mu}(x) = \ln \mu(x) \tag{3}$$

where $\mu(x)$ is the shear modulus which can be written in terms of elastic modulus as

$$\mu(x) = \frac{E(x)}{2(1+v)} \tag{4}$$

The fundamental solutions in Eq. (1) are expressed as [10]

$$U_{ij}(x,y) = \frac{1}{16\pi(1-v)r}\left[(3-4r)\delta_{ij} + r_i r_j\right] \tag{5}$$

$$T_{ij}(x,y) = -\frac{1}{8\pi(1-v)r^2}\times$$

$$\left[(1-2\nu)(n_i r_j - n_j r_i) + \big((1-2\nu)\delta_{ij} + 3r_i r_j\big)r_1 n_1\right] \tag{6}$$

$$V_{ij}(x,y) = -\frac{1}{8\pi(1-v)r^2}\times$$

$$\left[(1-2\nu)(\overline{\mu}_i r_j - \overline{\mu}_j r_i) + \big((1-2\nu)\delta_{ij} + 3r_i r_j\big)r_1 \overline{\mu}_1\right] \tag{7}$$

It is noteworthy that $U_{ij}(x,y)$ and $T_{ij}(x,y)$ are the essential solutions for the corresponding homogeneous, isotropic, and linear elastic solid [22,23], because such essential solutions are not yet available for general FGM. Eq. (1) gives the displacement at any internal point when f_j and are known at every boundary point and consequently when the boundary value problem is solved, the values at the internal points can be evaluated. However, since Eq. (1) is valid for every point in Ω including Γ, boundary domain integral equations can be obtained by letting $y \to \Gamma$ in Eq. (1), thus for boundary points Eq. (1) is written as below:

$$C_{ij}(y)\overline{u}_j(y) = \int_\Gamma U_{ij}(x,y) f_j(x) d\Gamma - \int_\Gamma T_{ij}(x,y)\overline{u}_j(x) d\Gamma$$

$$+ \int_\Omega V_{ij}(x,y)\overline{u}_j(x) d\Omega \tag{8}$$

where, $C_{ij}(y)$ is a Coefficient dependent on the local boundary geometry at point y.

3. Discretization and Solution of the BDI Equation

In order to solve the integral equations numerically, the boundary must be discretized into a series of elements over which displacements and tractions are written in terms of their values at a series of nodal points. The discretized form for the Eq. (1) without the domain integral is written as [24]

$$\overline{u}(y) = \sum_{j=1}^{NE}\left\{\int_{\Gamma_j} U^*(x(\xi,\eta),y) N(\xi,\eta) J(\xi,\eta) d\xi d\eta\right\} F^j$$

$$- \sum_{j=1}^{NE}\left\{\int_{\Gamma_j} T^*(x(\xi,\eta),y) N(\xi,\eta) J(\xi,\eta) d\xi d\eta\right\} U^j \tag{9}$$

where $U^* = [U_{ij}]$ and $T^* = [T_{ij}]$, U^j, F^j are the element nodal displacements and tractions in the element 'j' respectively, $N(\xi,\eta)$ is the matrix of shape functions, $J(\xi,\eta)$ is the Jacobean and (ξ,η) are the local coordinates. But this method cannot be applied on the domain integral in Eq. (1), in fact the main problem to the numerical solution of the boundary domain integral (BDI) equations is how to evaluate the domain integral in Eq. (1). One of the methods used for this purpose is the RIM of Gao [25,26], by this method the domain integral is transformed into the boundary integrals. It is observed that the direct transformation of domain integrals to the boundary is mathematically difficult. However, the direct transformation for domain integrals containing unknown quantities is unfeasible. So the normalized displacements in the domain integral of Eq. (1) must be estimated. For this purpose, the Radial Basic Functions are used [27]. Thus, the normalized displacements $\overline{u}(x)$ are approximated by

$$\overline{u}_i(x) = \sum_A \phi_i^A \varphi^A(R) + \phi_i^k x_k + \phi_1^0 \tag{10}$$

$$\sum_A \phi_i^A = 0 \tag{11}$$

$$\sum_A \phi_i^A x_j^A = 0 \tag{12}$$

where $R = |x - x^A|$ is the distance between point A, x, also, ϕ_i^A, ϕ_i^k are coefficients to be determined, and x^A denotes the coordinates at the application point A. The application points include all boundary nodes and some selected internal nodes. In this study, the following cubic Radial Basic Functions (RBFs) were used.

$$\varphi^A(R) = R^2 \tag{13}$$

The coefficients, φ_i^A and φ_i^k, in the above equations can be calculated by collocating the application point A in Eq. (10) at every node. A set of algebraic equations can be written together with Eqs. (11) and (12) in the matrix form as follows

$$\overline{u} = \varphi^{-1}\phi \tag{14}$$

where $\{\phi\}$ is a vector including the coefficients φ_i^A and φ_i^k at all application nodes $\{\overline{u}\}$ and is a vector including the values of the normalized displacements at all nodes. when no two nodes share the same coordinates, the matrix $[\varphi]$ is invertible and therefore

$$\phi = \varphi\overline{u} \tag{15}$$

Using Eq. (10), the domain integrals consisting of $V_{ij}, \overline{u}_j$ can be written as:

$$\int_\Omega V_{ij}(x,y)\overline{u}_j(x) d\Omega = \sum_A \phi^A \int_\Omega V_{ij}(x,y)\Phi^4 d\Omega$$

$$+ \phi^k \int_\Omega V_{ij}(x,y) x_k d\Omega + \phi^0 \int_\Omega V_{ij}(x,y) d\Omega \tag{16}$$

The integrals of Eq. (16) using RIM can be transformed into boundary integrals as follows:

$$\int_{\Omega} V_{ij}(x,y)\overline{u}(x)d\Omega = \sum_{A} \phi^{A} \int_{\Gamma} \frac{F^{A}(x,y)}{r^{\phi}(x,y)} \frac{\partial r}{\partial n} d\Gamma$$

$$+ \phi^{k} \int_{\Omega} \frac{r_k F^{1}_{ij}(x,y)}{r^{\phi}(x,y)} \frac{\partial r}{\partial n} d\Gamma + (\phi^{k} x_k + \phi^{0}) \int_{\Gamma} \frac{F^{0}_{ij}(x,y)}{r^{\phi}(x,y)} \frac{\partial r}{\partial n} d\Gamma \quad (17)$$

where

$$F^{A}_{ij} = \int_{0}^{r} r^2 V_{ij} \varphi^{A} dr \quad (18)$$

$$F^{1}_{ij} = \int_{0}^{r} r^3 V_{ij} dr \quad (19)$$

$$F^{0}_{ij} = \int_{0}^{r} r^2 V_{ij} dr \quad (20)$$

Since F^A is the function of the distance R, F^A needs to be first expressed in terms of r, the distance from the source point p to the field point Q, which can be written as

$$R = \sqrt{r^2 = sr + \overline{R}^2} \quad (21)$$

where

$$s = 2r_i\overline{R}_i, \quad \overline{R} = ||y - x^A|| = \sqrt{\overline{R}_i\overline{R}_i}, \quad \overline{R}_i = y_i - x^A_i \quad (22)$$

It should be noted that the integral singularities in the domain integral will be removed using the RIM [19]. By applying Eqs. (1) and (8) at all internal and boundary points respectively and after considering the boundary conditions the following system of linear algebraic equations is produced [10]. It is assumed that the BEM model includes N_b and N_i.

$$A_b \cdot x_b = y_b + V_b \cdot \overline{u} \quad \text{(The boundary nodes)} \quad (23)$$

$$\overline{u}_i + A_i \cdot x_b = y_i + V_i \cdot \overline{u} \quad \text{(The internal nodes)} \quad (24)$$

where $\overline{u}$ is consisting of the unknown normalized boundary displacements with all normalized internal displacement and x_b is consisting of the unknown normalized boundary displacements (the unknown boundary traction). To solve system of equations it needs to express it in the following form [10]

$$\left(\begin{bmatrix} A_b & 0 \\ -A_i & I \end{bmatrix} - \begin{bmatrix} V_b \\ V_i \end{bmatrix} \right) \begin{Bmatrix} x_b \\ \overline{u}_i \end{Bmatrix} = \begin{Bmatrix} y_b \\ y_i \end{Bmatrix} \quad (25)$$

where $\overline{u}_i$ is consisting of the normalized internal displacements. When Eq. (25) is solved numerically, it gives the boundary and internal values. To obtain the true displacements, Eq. (2) is used.

4. SIF Evaluation

Considering the asymptomatic crack-tip field for continuously non-homogeneous, isotropic and LES, the SIFs can be obtained from crack opening displacements (CODs) as [27,28],

$$\begin{Bmatrix} K_I \\ K_{II} \\ K_{III} \end{Bmatrix} = \frac{\mu_{tip}\sqrt{2\pi}}{4(1-v)} \lim_{\delta \to 0} \frac{1}{\sqrt{\delta}} \begin{Bmatrix} \Delta u_{\xi}(\delta) \\ \Delta u_{\eta}(\delta) \\ (1-v)\Delta u_{\gamma}(\delta) \end{Bmatrix} \quad (26)$$

where the K_I and K_{II} are opening and shearing modes SIF, Δu_{ξ}, Δu_{η} and Δu_{γ} are the CODs in the local coordinate system, is a distance of the node on the crack surface from the crack front, is the shear modulus at the crack-front.

5. Numerical Analysis and Results

As shown in Fig. 1, an internal longitudinal semi-elliptical surface crack in an FGM pressurized thick-walled cylinder is loaded under internal pressure. The crack geometry is followed by two dimensionless parameters, the aspect ratio (a/c) and relative depth of crack (b/t), as shown in Fig. 2.

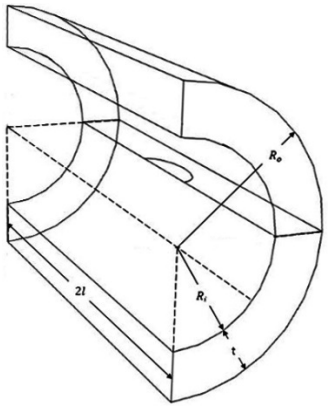

Fig. 1. Semi-elliptical surface crack in an FGM pressurized thick-walled cylinder.

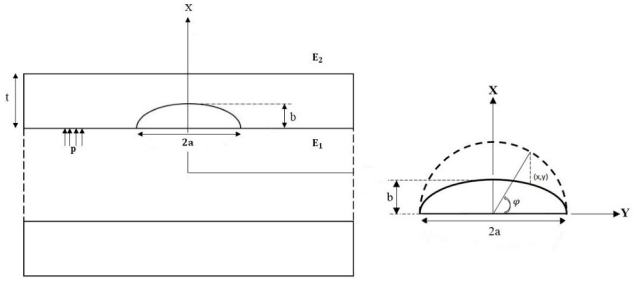

Fig. 2. The geometry parameters of semi-elliptical surface crack in an FGM pressurized cylinder.

The elastic modulus is calculated by an exponential law:

$$E(r) = E_1 e^{\beta(r-R_i)} \quad (27)$$

where β defined as:

$$\beta = t^{-1} \ln\left(\frac{E_2}{E_1}\right) \tag{28}$$

For simplification, in this study, the Poisson's ratio is assumed constant throughout the cylinder and it is taken as $v = 0.25$. For all geometries, the ratio of crack length to cylinder length (a/l) equal to 0.1. Because of the symmetry, only 1/4 of the cylinder needs to be discretized. For the vessel boundary, 8-node quadrilateral boundary elements are used. The used BEM mesh is illustrated in Fig. 3. At the crack-front, discontinuous 8-node quadrilateral boundary elements are adopted as shown in Fig. 4.

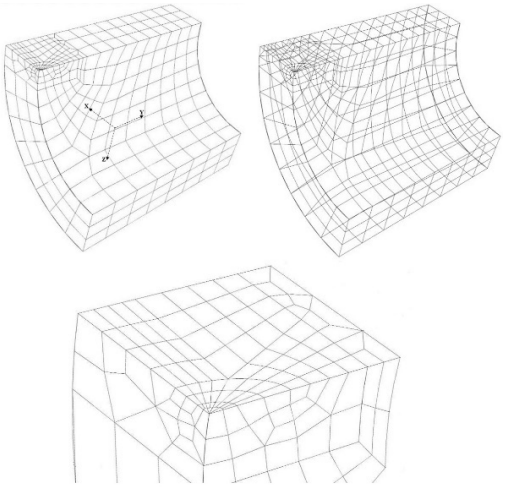

Fig. 3. BE model and discretization of the crack-surface.

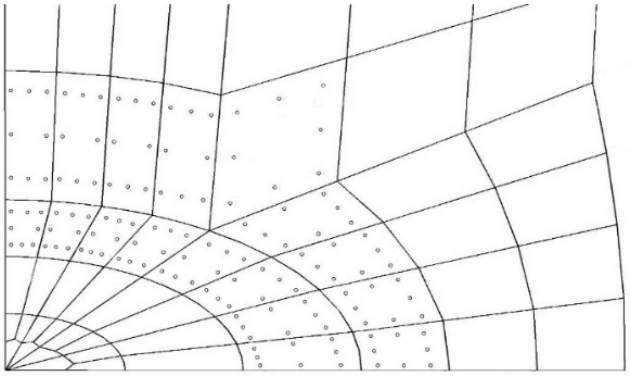

Fig. 4. Discontinuous 8-noded quadrilateral elements at the crack front.

5.1. Boundary Conditions

Symmetry boundary conditions are applied to the $X = 0$, $Y = 0$, $Z = 0$ and the $Y = l$ plane is constrained in the Y-direction and internal pressure is applied to the crack surfaces as shown in Fig. 5 that is symmetric about the $Z = 0$ plane. The element numbers are 451, the total node numbers on boundary are 1355 and the internal nodes numbers are 250. The analyses were carried out by MATLAB codes. The $\overline{K}_I$ are shown in the Figs. 6a-6d and follow as:

$$\overline{K}_I = \frac{K_I}{K_0} \tag{29}$$

in which K_0, Q is approximated by

$$K_0 = \frac{PR_i}{t}\sqrt{\frac{\pi b}{Q}} \tag{30}$$

$$Q = 1 + 1.464\left(\frac{b}{a}\right)^{1.65} \tag{31}$$

Moreover, the normalized values for CTOD in direction of crack regime for cylinder of FGM with $t/R_i = 0.5$, $b/a = 0.5$ and $b/t = 0$ is illustrated in Fig. 7. It is provided that the maximum SIF occurred in $\varphi = 0$, therefore, the study of effect of the gradient of the SIF at this points is important. Fig. 8 shows SIF versus material gradient at $\varphi = 0$. For study effect of pressure, K_I in several pressures is calculated in $\varphi = 90$, whose results are shown for homogenous vessel and FGM with several of material gradient in Fig. 9.

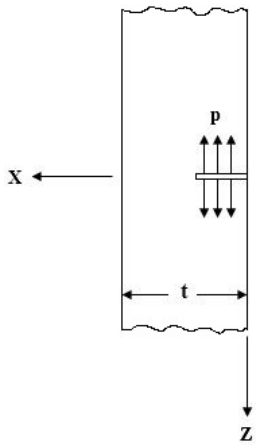

Fig. 5. A semi-elliptical surface crack in a cylinder under loading.

In this study, a semi-elliptical surface crack was assumed in an FGM thick-walled cylindrical pressure vessel under internal pressure. The Poisson's ratio was considered to be constant with a value of 0.25 throughout the cylinder. The K_I as a function of φ for an FGM and corresponding homogeneous cylinder, are shown in Figs. 6a-6d. For homogeneous cylinder, the obtained results were compared with those reported by Chai Guozhong et al. [28] and good agreement for both cases was observed. Different values of relative depths of crack and material gradients (E_2/E_1) were applied. The ratio of wall thickness to cylinder inner radius was 0.5, the aspect ratio was 0.5, the analyzed relative depth of crack ranged from 0.2 to 0.8 and the material gradient was 0.2, 5 and 10.

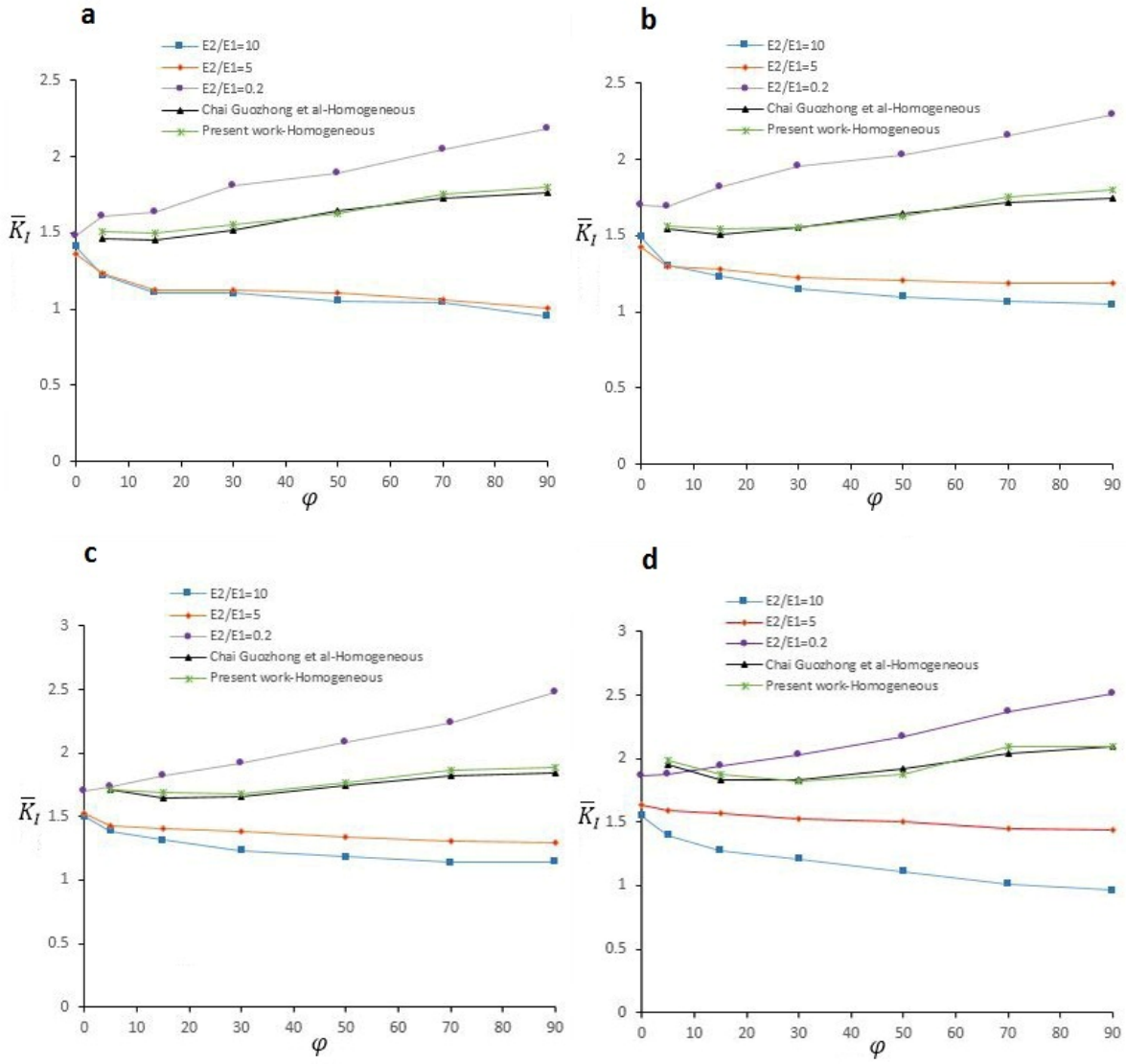

Fig. 6. The along the crack front with $t/Ri = 0.5, b/a = 0.5$ and different values of the crack depths; a) $b/t = 0.2$; b) $b/t = 0.4$; c) $b/t = 0.6$; d) $b/t = 0.8$.

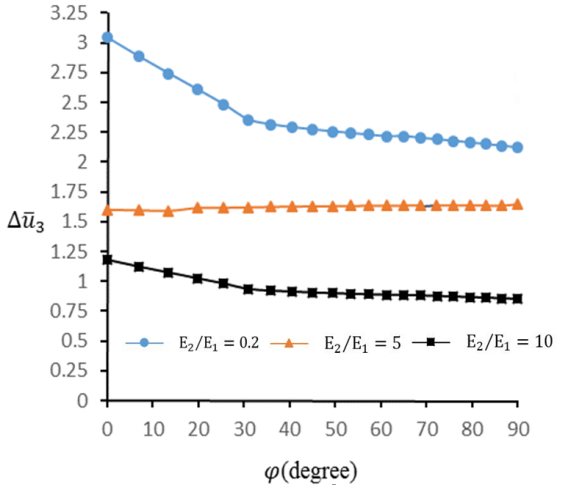

Fig. 7. A semi-elliptical surface crack in a cylinder under Loading.

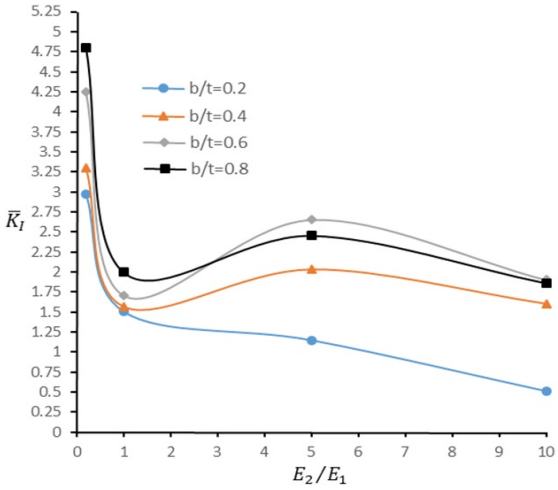

Fig. 8. The $\overline{K}_I$ versus material gradient at $\varphi = 0$.

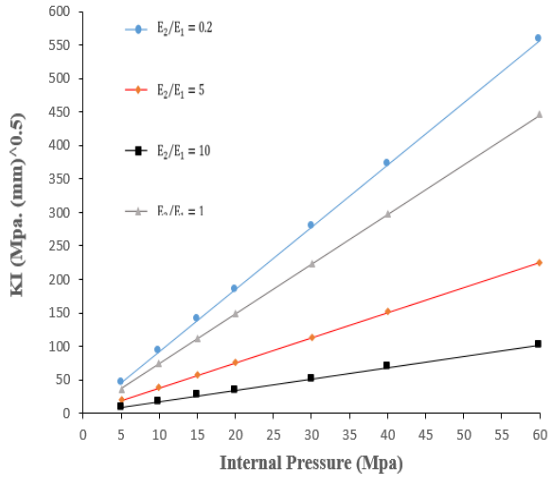

Fig. 9. The K_I versus internal pressure of vessel in $b/t = 0.2$ (BEM).

6. Vessel Modeling in Software

For modeling and analysis of vessel, XFEM in ABAQUS software was applied and due to symmetrical geometry and loading, a quarter of vessel was applied to appropriate boundary conditions; the elastic modulus and Poissons ratio were considered. Assembled model with crack is shown in Fig. 10.

Fig. 10. Internal pressure and boundary conditions on model.

It is important that in the models with crack, elements in crack tip should be small enough to be chosen. Therefore, to increase accuracy, meshing size around crack region must be fine and for other points on vessel, coarse mesh was considered. Figs. 11, 12 show mesh around crack and applied internal pressure and boundary conditions. In this section, the K_I was investigated in several points on crack regime. The SIF parameter was calculated for nodes located on stress regime. Applied force in this procedure, was statically force with 0.1 second step time. Also, total time for analyses was equal to 1 second. In the present research, the analysis of nonlinear static was considered. The FGM properties were programmed in MATLAB software. The obtained numerical results for stress and displacement Countors are shown in Figs. 13, 14.

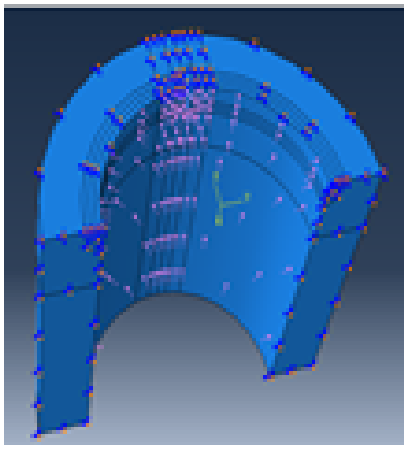

Fig. 11. Internal pressure and boundary conditions on model.

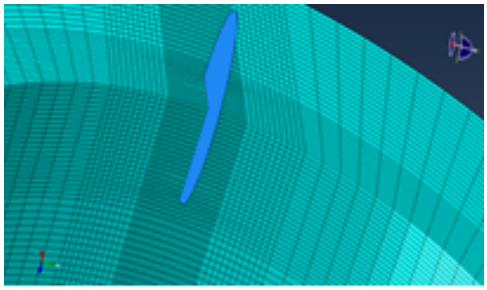

Fig. 12. Meshing around crack in vessel.

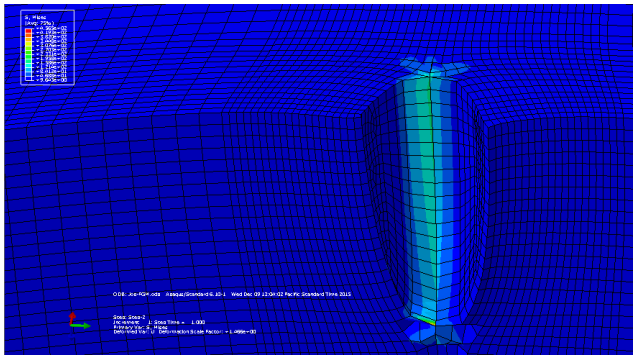

Fig. 13. The Von Mises stress countor around crack tip.

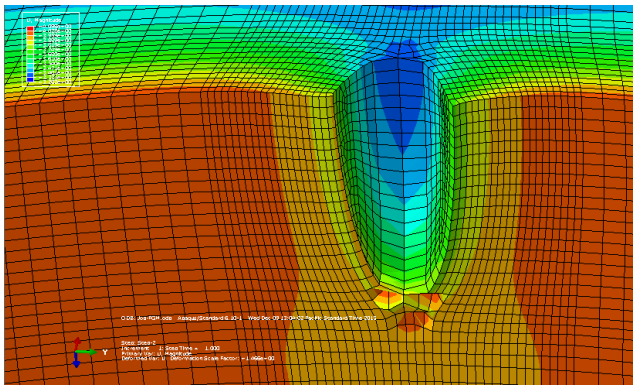

Fig. 14. The displacement countor around crack tip.

The ABAQUS software numerical analysis is based

on finite element method, and the accuracy of the method depends on the convergence of the meshing, the element type, and the degrees of freedom of nodes. But in boundary element method, for numerical analysis the integral equation governing the system and the boundary of system must be discretized into a series of elements, so for each element displacement and surface forces are determined based on the number of nodal points. If the discrete form of governing equation is written for each node at the boundary, then a linear equations of system is obtained, which by applying boundary conditions, these equations can be solved and unknown values are determined.

In extended FEM, phantom nodes are used for analysis of fracture, which were assigned no displacement or any other physical variables and so became, in eect, just extra storage space for the physical nodes with no reection in reality [29].

Due to the advantages of extended finite element method in crack analysis, and also, the simplicity and non-limitation of this method, therefore, in present research, for functional graded material analysis, XFEM was selected. In the numerical analysis of vessel, it was tried tried to create the fine mesh size so that the answers converge enough, also, the results for homogeneous vessel compared to the results of Guozhong et al. [28] show that the same dimensions and specifications were selected. The obtained results for two studies had good agreement, so the mesh size was considered to be the same for the functional graded material. Considering that this present research was conducted for the first time for FGM pressure vessel, therefore, there was no reference for $E_2/E_1 = 1.0$, steel homogenous vessel (the normalized SIF on crack regime versus φ). the obtained results from ABAQUS software were compared to Guozhong et al. results and it is shown in Table. 1. Also, the SIF on crack regime versus φ for different internal pressure is illustrated in Table 2.

The ratio thickness for internal radius of vessel was equal to 0.5 and crack relative depth, the values of 0.2-0.8 with increment of 0.2 and also the manner of material distribution was equal to 0.2, 5, 10. The numerical results indicate that maximum SIF take place in $\varphi = 0$, and the effect of internal pressure on SIF for $E_2/E_1 = 0.2, 1, 5, 10$ is shown in Fig. 15. Also, the normalized K_I versus for FE and BE methods are shown in Figs. 16-19.

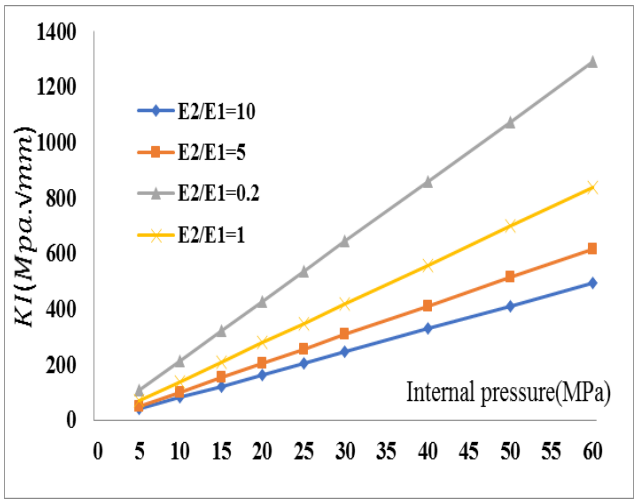

Fig. 15. $\overline{K_I}$ in direction of crack regime, $b/t = 0.2$, $b/a = 0.5$, $t/R_i = 0.5$. (FEM)

Table 1
Comparison of the normalized SIF on crack regime versus φ.

	b/t							
φ	0.2		0.4		0.6		0.8	
	Guozhong	ABAQUS	Guozhong	ABAQUS	Guozhong	ABAQUS	Guozhong	ABAQUS
5	1.464	1.226	1.541	1.303	1.476	1.714	1.950	1.712
10	1.450	1.250	1.506	1.306	1.445	1.645	1.837	1.637
30	1.518	1.354	1.550	1.356	1.467	1.661	1.887	1.633
50	1.645	1.425	1.650	1.428	1.525	1.747	1.924	1.702
70	1.731	1.465	1.720	1.454	1.550	1.816	2.039	1.773
90	1.760	1.489	1.743	1.472	1.571	1.842	2.100	1.829

Table 2
The SIF on crack regime versus for different internal pressure (The obtained results ABAQUS software).

	Internal Pressure (Mpa)					
φ	5	10	15	20	25	30
5	30.30342	60.60683	90.91025	121.2137	151.5171	181.8205
10	30.01363	60.02726	90.04089	120.0519	150.0681	180.0818
30	31.42116	62.84233	94.26319	125.6847	157.1056	188.5270
50	34.04994	68.09989	102.1428	136.1998	170.2497	204.2997
70	35.83006	71.66013	107.4902	143.3203	179.1503	214.9804
90	36.43034	72.86067	109.2910	145.7213	182.1517	218.5820

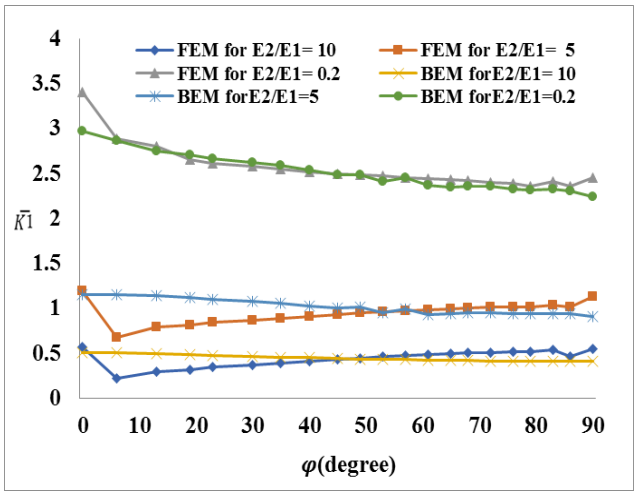

Fig. 16. Comparison of $\overline{K_I}$ in direction of crack regime, $b/t = 0.2,\ b/a = 0.5,\ t/R_i = 0.5$.

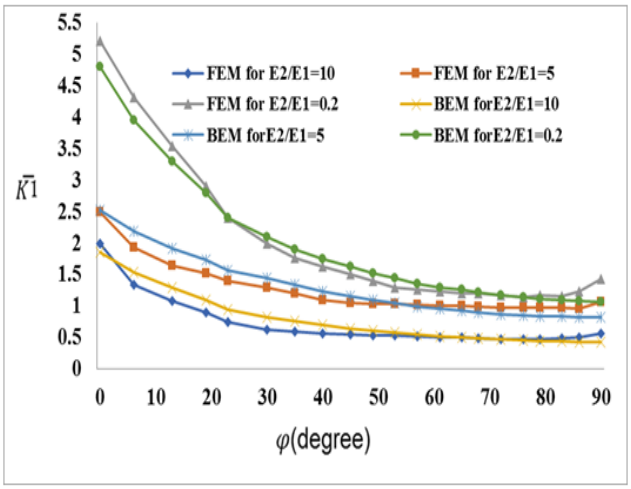

Fig. 17. Comparison of $\overline{K_I}$ in direction of crack regime, $b/t = 0.8,\ b/a = 2,\ t/R_i = 0.5$.

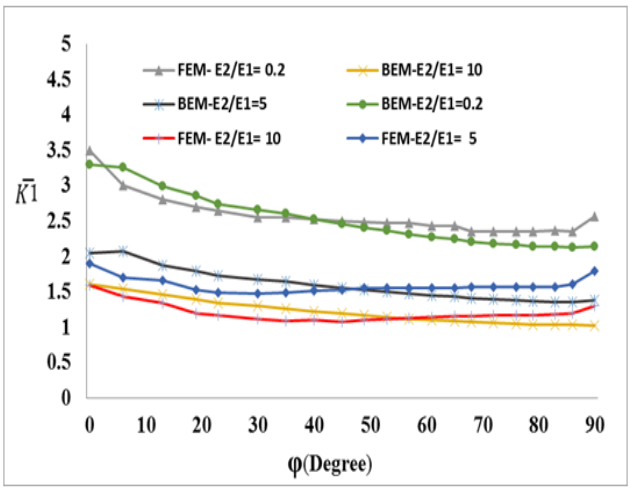

Fig. 18. Comparison of $\overline{K_I}$ in direction of crack regime, $b/t = 0.4,\ b/a = 1,\ t/R_i = 0.5$.

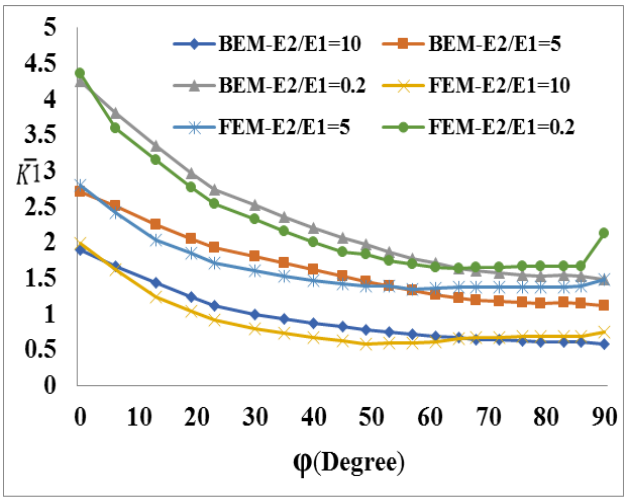

Fig. 19. Comparison of $\overline{K_I}$ in direction of crack regime, $b/t = 0.6,\ b/a = 1.5,\ t/R_i = 0.5$.

7. Conclusions

One of the most important applications of FGM is as initial material in the manufacturing of vessels. Fracture study is very important in FGM vessels because of various usage in different industries. Since these vessels could have cracks that have been occurred during the manufacturing process, there is often fracture probability. One of the important parameters in fracture study is estimation of SIF, which is a controllable parameter in evaluation of the critical state of crack. In the present work, a semi-elliptical surface crack in an FGM thick-walled cylindrical vessel under internal pressure was assumed. The Poisson's ratio was constant throughout the vessel and the material properties were considered to be isotropic with linear elastic behavior.

The elastic modulus varies exponentially in the radial direction. The opening mode SIF is estimated by the boundary element method with different values of crack depths and crack lengths which all equations have been programmed in MATLAB software. Because of non-homogeneous nature of FGM, the boundary element formulation contains the domain integral. To transform the domain integral into boundary integrals, a meshless method was applied, which doesn't require the discretization of vessel but it needs additional interior nodes instead of interior cells or meshes. Finally, effect of internal pressure, the manner of material distribution and crack geometry on K_I were studied. In the present study, the following conclusions were drawn:

1. The obtained results illustrate that increase in the E_2/E_1, decreases SIF and when $E_2/E_1 = 10$, the SIF of the FGM vessel is always lower than the corresponding homogeneous vessel.

2. As the relative depth of crack b/t increases, the decreasing trend of SIF comparative to Parametric angle (φ) is increases.

3. In FGM vessel, the maximum SIF occurs at corner points of crack ($\varphi = 0$) while for homogeneous vessel, the critical point of SIF is often at the deepest point ($\varphi = 90$).

4. The relationship between SIF and internal pressure in functional graded material is linear, so that increasing internal pressure increases SIF linearity.

5. Since the crack growth starts from the point which has maximum SIF, so it can be said that the corner points in this vessel, are critical points. Finally, it could be claimed that a good agreement was observed between two methods

6. In accordance with Table 2, the SIF increases with increasing internal pressure of the vessel at different φ, except in $\varphi = 10$. The obtained results show that internal pressure of vessel compared to has a notable effect on the SIF.

7. In Fig. 9, when internal pressure increases, with increasing material gradient, the K_I decreased. Also, the relation between K_I and internal pressure for different material gradient is linear.

8. For study of effect crack geometry, in Fig. 8, for $b/t = 0.2, 0.4, 0.6$ and 0.8 by increasing material gradient from 5 to 10, the normalized K_I decreases and $b/t = 0.2$ is expected as the normalized K_I increases.

9. In Fig. 19, the normalized K_I in direction of crack regime, $b/t = 0.6$, $b/a = 1.5$, $t/R_i = 0.5$, for all of the material gradients by increasing φ decreases.

References

[1] R. Seifi, Stress intensity factors for internal surface cracks in autofrettaged functionally graded thick cylinders using weight function method, Theor. Appl. Fract. Mech., 75 (2015) 113-123.

[2] I. Eshraghi, N. Soltani, Stress intensity factor calculation for internal circumferential cracks functionally graded cylinders using the weight function approach, Eng. Fract. Mech., 134 (2015) 1-19.

[3] A. Shaghaghi-Moghaddam, M. Alfano, M. Ghajar, Determining the mixed mode stress intensity factors of surface cracks in functionally graded hollow cylinders, Mater. Des., 43 (2013) 475-484.

[4] A.M. Afsar, M. Anisuzzaman, Stress intensity factors of two diametrically opposed edge cracks in a thick-walled functionally graded material cylinder, Eng. Fract. Mech., 74 (2007) 1617-1636.

[5] Y. Ootao, R. Kawamura, Y. Tanigawa, R. Imamura, Optimization of material composition of nonhomogeneous hollow sphere for thermal stress relaxation making use of neural network, Comput. Meth. Appl. Mech. Eng., 180 (1999) 185-201.

[6] Y. Ootao, R. Kawamura, Y. Tanigawa, R. Imamura, Optimization of material composition of nonhomogeneous hollow circular cylinder for thermal stress relaxation making use of neural network, J. Thermal. Stress., 22 (1999) 1-22.

[7] A.R. Saidi, S.R. Atashipour, E. Jomehzadeh, Exact elasticity solutions for thick- walled FG spherical pressure vessels with linearly and exponentially varying properties, Int. J. Eng., Transactions A: Basics, 22(4) (2009) 405-416.

[8] M.H. Heydari, N. Choupani, A new comparative method to evaluate the fracture properties of laminated composite, Int. J. Eng., Transactions C: Aspects, 27(6) 991-1004.

[9] A.R. EL-Desouky, M.S. EL-Wazery, Mixed mode crack propagation of zirconia/nickel functionally graded materials, Int. J. Eng.,Transactions B: Application, 26(8) (2013) 885-894.

[10] C.H. Zhang, M. Cui, J.Wang, X.W. Gao, J. Sladek, V. Sladek, 3D crack analysis in functionally graded materials, Eng. Fract. Mech., 78 (2011) 585-604.

[11] J.L. Wearing, S.Y. Ahmadi-Brooghani, the evaluation of stress intensity factors in plate bending problems using the dual boundary element method, Eng. Anal. Bound. Element., 23 (1999) 3-19.

[12] J.P. Pereira, C.A. Duarte, Extraction of stress intensity factors from generalized finite element solutions, Engin. Anal. Bound. Element., 29 (2005) 397-413.

[13] J. Purbolaksono, A.A. Ali, A. Khinani, A.Z. Rashid, Evaluation of stress intensity factors for multiple surface cracks in bi-material tubes, Eng. Anal. Bound. Element., 33(11) (2009) 1339-1343.

[14] A. Barroso, E. Graciani, V. Mantic, F. Paris, A least squares procedure for the evaluation of multiple generalized stress intensity factors at 2D multimaterial corners by BEM, Eng. Anal. Bound. Element., 36 (2012) 458-470.

[15] I.A. Alatawi, J. Trevelyan, A direct evaluation of stress intensity factors using the Extended Dual Boundary Element Method, Eng. Anal. Bound. Element., 52 (2015) 56-63.

[16] N. Tutuncu, M. Ozturk, Exact Solution for stresses in functionally graded pressure vessels, Composites, part B, 32 (2001) 683-686.

[17] C.O. Horgan, A.M. Chan, The pressurized hollow cylinder or disk problem for functionally graded isotropic linearly elasticity, J. Elast., 55 (1999) 43-59.

[18] M. Jabbari, S. Sohrabpour, M.R. Eslami, Mechanical and thermal stresses in a functionally graded hollow cylinder due to radially symmetric loads, Int. J. Pres. Ves. Pip., 79 (2002) 493-497.

[19] A. Ghasemi, A. Kazemian, M. Moradi, Analytical and numerical investigation of FGM pressure vessel reinforced by laminated composite materials, J. Sol. Mech., 6(1) (2014) 43-53.

[20] Y. Chen, X. Lin, Elastic analysis for thick cylinders and spherical pressure vessels made of functionally graded materials, Comput. Mater. Sci., 44(2) (2008) 581-587.

[21] K. Abrinia H. Naee, F. Sadeghi, F. Djavanroodi, New analysis for the FGM thick cylinders under combined pressure and temperature loading, American J. Appl. Sci., 5(7) (2008) 852-859.

[22] M.H. Aliabad, The Boundary Element Method: Applications in solids and structures, 2, John Wiley & Sons, (2002).

[23] X.W. Gao, T.G. Davies, Boundary Element Programming in Mechanics, Cambridge University Press, (2002).

[24] C.A. Brebbia, J. Dominguez, Boundary Elements an Introductory Course, McGraw Hill, New York, NY, (1989).

[25] X.W. Gao, The radial integration method for evaluation of domain integrals with boundary-only discretization, Eng. Anal. Bound. Element., 26 (2002) 905-916.

[26] X.W. Gao, A boundary element method without internal cells for two-dimensional and three dimensional elastoplastic problems, J. Appl. Mech., 69 (2002) 154-60.

[27] J.W. Eischen, Fracture of nonhomogeneous materials, Int. J. Fract., 34 (1987) 3-22.

[28] C. Guozhong, Z. Kangda, W.U. Dongdi, Stress intensity factors for internal semi- elliptical surface cracks in pressurized thick-walled cylinders using the hybrid boundary element method, Eng. Fract. Mech., 52 (1995) 1055-1064.

[29] M.J. McNary, Implementation of the extended finite element method (XFEM) in the ABAQUS software package, MSc. Thesis in mechanical engineering, Georgia Institute of Technology, (2009).